Direct measurement of quantum geometric tensor in pseudo-Hermitian systems

Ze-Hao Huang,[1, 2, *] Hai-Tao Ding,[3, 4, †] and Li-Jun Lang[5, 6, ‡]

[1]*National Laboratory of Solid State Microstructures and School of Physics, Nanjing University, Nanjing 210093, China*
[2]*Collaborative Innovation Center of Advanced Microstructures, Nanjing University, Nanjing 210093, China*
[3]*Centre for Quantum Technologies, National University of Singapore, 3 Science Drive 2, Singapore 117543*
[4]*MajuLab, CNRS-UNS-NUS-NTU International Joint Research Unit, Singapore UMI 3654, Singapore*
[5]*Guangdong Basic Research Center of Excellence for Structure and Fundamental Interactions of Matter,*
Guangdong Provincial Key Laboratory of Quantum Engineering and Quantum Materials,
School of Physics, South China Normal University, Guangzhou 510006, China
[6]*Guangdong-Hong Kong Joint Laboratory of Quantum Matter,*
Frontier Research Institute for Physics, South China Normal University, Guangzhou 510006, China

(Dated: September 23, 2025)

The quantum geometric tensor (QGT) fundamentally encodes the geometry and topology of quantum states in both Hermitian and non-Hermitian regimes. While adiabatic perturbation theory links its real part (quantum metric) and imaginary part (Berry curvature) to energy fluctuations and generalized forces, respectively, in Hermitian systems, direct measurement of the QGT, which defined using both left and right eigenstates of non-Hermitian Hamiltonian, remains challenging. Here we develop two quantum simulation schemes to directly extract all components of the QGT in pseudo-Hermitian systems with real spectra. Each scheme independently determines the complete QGT using generalized expectation values of either the energy fluctuation operator or the generalized force operator with respect to two time-evolved states prepared through distinct nonadiabatic evolutions, thereby establishing two self-contained measurement protocols. We illustrate the validity of these schemes on two q-deformed 2-band models: one with nontrivial topology, and the other with a nonvanishing off-diagonal quantum metric. Numerical simulations show that both schemes achieve high-fidelity agreement with theoretical predictions for measuring the QGT of both models, and successfully capture the topological phase transition of the first model using Chern numbers calculated from Berry curvatures. This work provides a framework for extending dynamical measurement schemes from Hermitian to pseudo-Hermitian systems with real spectra.

I. INTRODUCTION

The quantum geometric tensor (QGT) [1–3] is a fundamental quantity in quantum mechanics, characterizing the geometric and topological properties of quantum systems. Its symmetric real part, known as the quantum metric tensor (QMT) [4], quantifies the quantum distance and Fisher information [5] in parameter space and governs phenomena including flat-band superfluidity [6–8], orbital magnetic susceptibility [9, 10], and the nonlinear Hall effect [11–13]. The antisymmetric imaginary part, which corresponds to the Berry curvature [14], determines the geometric phase [15, 16] and topological invariants such as the Chern number [17] for topological quantum matter [18–22]. Both components serve to characterize quantum phase transitions [23–26]. Alongside theoretical progress in generalizing the QGT from its original Abelian forms for pure states in nondegenerate systems to non-Abelian forms in degenerate systems [27, 28] and to mixed states [29–31], experimental advances have enabled its measurement across diverse platforms, including superconducting qubits [32–38], ultracold atoms [39–45], nitrogen-vacancy (NV) centers [46–48], exciton-photon polaritons [49], and, most recently, solid-state systems [50].

Unique phenomena revealed in non-Hermitian systems beyond Hermitian ones [51–53] have motivated the generalization of the QGT to non-Hermitian systems, thereby yielding two alternative definitions: the right-right (RR) formalism defined using only right eigenstates [54–57], and the left-right (LR) formalism defined using both left and right eigenstates [58–67]. Both formalisms of the QGT play crucial roles in wavepacket dynamics [68–70]. While the Berry curvature in both formalisms characterizes the same topological phases through identical Chern numbers obtained from its integration over the Brillouin zone [71], the QMT exhibits distinct roles: specifically, the RR formalism identifies localization transitions [57], whereas the LR formalism detects quantum phase transitions [59–61] and exceptional points [62, 63]. Experimentally, despite successful demonstrations of the RR formalism [72–74], the QGT in LR formalism has not yet been measured. We therefore focus exclusively on the LR formalism hereafter.

Pseudo-Hermitian systems, representing a special class of non-Hermitian systems whose spectra are either purely real eigenvalues or complex-conjugate pairs [75–78], have stimulated considerable interest due to their dynamical analogies to Hermitian systems [79] and novel properties such as enhanced quantum sensing [80]. Measuring the QGT in pseudo-Hermitian systems with real spectra is still an important experimental challenge. While Ref. [65]

_____

[*] zhhuang98@smail.nju.edu.cn
[†] htding.9@nus.edu.sg
[‡] ljlang@scnu.edu.cn

proposed an indirect approach using Rabi frequencies, practical schemes for direct measurement of the QGT are essential to advance experimental studies.

We develop two independent schemes for direct measurement of the QGT in pseudo-Hermitian systems with real spectra. Our schemes integrate adiabatic perturbation theory for describing time-dependent dynamics [81–84] with quantum circuits that implement the measurement of expectation values of an operator with respect to two states [85–87], dubbed generalized expectation values, whose form is similar to weak values [88–90]. The first scheme extracts both real and imaginary parts of QGT by measuring generalized expectation values of the energy fluctuation operator $\Delta^2 H \equiv (H - \langle H \rangle)^2$ within a unified experimental framework. The second scheme utilizes the generalized force operator $f_\mu \equiv -\partial_\mu H$ and requires two distinct measurements of generalized expectation values to separately obtain the real and imaginary parts of QGT. We verify the two schemes using two pseudo-Hermitian q-deformed 2-band models: one with nontrivial topology and the other with a nonvanishing off-diagonal quantum metric. Numerical results demonstrate high-fidelity QGT measurement for both schemes. Remarkably, for the first model, the Chern number phase diagram can be built up accurately through both generalized force and energy fluctuation schemes, contrasting with Hermitian systems where only the generalized force approach is available [32].

The paper is structured as follows. In Sec. II, we introduce the QGT in LR formalism for non-Hermitian systems and demonstrate its reduction to a Hermitian quantity under the pseudo-Hermiticity constraint with real spectra. In Sec. III, we present two distinct schemes for measuring the complete QGT in such systems. Numerical verification via two illustrative examples appears in Sec. IV. In Sec. V, we discuss experimental implementations. Concluding remarks are provided in Sec. VI.

II. QUANTUM GEOMETRIC TENSOR IN PSEUDO-HERMITIAN SYSTEMS

We consider a generic N-band non-Hermitian Hamiltonian $H(\boldsymbol{\lambda})$ parameterized by $\boldsymbol{\lambda} = (\lambda_1, \lambda_2, \cdots)$. The time-independent Schrödinger equations are given by:

$$H(\boldsymbol{\lambda})|\phi_n^R(\boldsymbol{\lambda})\rangle = E_n(\boldsymbol{\lambda})|\phi_n^R(\boldsymbol{\lambda})\rangle, \quad (1)$$

$$H^\dagger(\boldsymbol{\lambda})|\phi_n^L(\boldsymbol{\lambda})\rangle = E_n^*(\boldsymbol{\lambda})|\phi_n^L(\boldsymbol{\lambda})\rangle, \quad (2)$$

yielding right eigenstates $|\phi_n^R(\boldsymbol{\lambda})\rangle$ and left eigenstates $|\phi_n^L(\boldsymbol{\lambda})\rangle$ that satisfy the biorthogonal relation $\langle \phi_i^L(\boldsymbol{\lambda})|\phi_j^R(\boldsymbol{\lambda})\rangle = \delta_{ij}$ [91]. Here, $E_n(\boldsymbol{\lambda})$ denotes discrete nondegenerate eigenvalues, with n indexing the energy bands.

For such systems, the quantum geometric tensor (QGT), constructed using both left and right eigenstates,

for n-th band is defined as [59, 61, 65]:

$$\begin{aligned} Q_{\mu\nu}^n &:= \langle \partial_\mu \phi_n^L | \partial_\nu \phi_n^R \rangle - \langle \partial_\mu \phi_n^L | \phi_n^R \rangle \langle \phi_n^L | \partial_\nu \phi_n^R \rangle \\ &= \sum_{m \neq n} \langle \partial_\mu \phi_n^L | \phi_m^R \rangle \langle \phi_m^L | \partial_\nu \phi_n^R \rangle, \end{aligned} \quad (3)$$

where $\partial_\mu \equiv \partial/\partial \lambda_\mu$, and $|\phi_n^{R,L}\rangle \equiv |\phi_n^{R,L}(\boldsymbol{\lambda})\rangle$ for notational simplicity.

In arbitrary non-Hermitian systems, the QGT is generally non-Hermitian ($Q_{\mu\nu}^n \neq (Q_{\nu\mu}^n)^*$), rendering the definitions of the quantum metric and Berry curvature ambiguous [61]. However, in pseudo-Hermitian systems with real spectra, which satisfy the pseudo-Hermiticity condition $H^\dagger = \eta H \eta^{-1}$ where η is a Hermitian invertible operator, the eigenstate relation $|\phi_n^L(\boldsymbol{\lambda})\rangle = \eta|\phi_n^R(\boldsymbol{\lambda})\rangle$ restores the Hermiticity of the QGT. Analogously to Hermitian systems, pseudo-Hermitian systems with real spectra admit unique definitions of the quantum metric $g_{\mu\nu}^n = \frac{1}{2}\left[Q_{\mu\nu}^n + (Q_{\nu\mu}^n)^*\right]$ and Berry curvature $F_{\mu\nu}^n = i\left[Q_{\mu\nu}^n - (Q_{\nu\mu}^n)^*\right]$.

III. DIRECT MEASUREMENT SCHEMES

In this section, we propose two schemes to directly measure the QGT component $Q_{\mu\nu}^0(\boldsymbol{\lambda}_{\text{tar}})$ for the lowest band at a target parameter $\boldsymbol{\lambda}_{\text{tar}}$ in pseudo-Hermitian systems with real spectra. We first discuss the state evolution used to prepare the time-evolved states, which is based on adiabatic perturbation theory (See Appendix A for details) [81–84]. Then, we describe how to select a pair of time-evolved states to construct the generalized expectation value of either the energy fluctuation operator $\Delta^2 H \equiv (H - \langle H \rangle)^2$ or the generalized force operator $f_\mu \equiv -\partial_\mu H$ for measuring the QGT. The generalized expectation value is defined as

$$\frac{\langle \psi_1 | A | \psi_2 \rangle}{\langle \psi_1 | \psi_2 \rangle}, \quad (4)$$

where A is an arbitrary operator, $|\psi_1\rangle$ and $|\psi_2\rangle$ are two arbitrary states.

State Evolution. We prepare the state $|\psi_\mu(\boldsymbol{\lambda}_{\text{tar}}, t)\rangle$ by evolving the initial state $|\psi_\mu(\boldsymbol{\lambda}_{\text{tar}}, 0)\rangle = |\phi_0^R(\boldsymbol{\lambda}_{\text{tar}} - \Delta\lambda \mathbf{e}_\mu)\rangle$ under the time-dependent Hamiltonian $H[\boldsymbol{\lambda}(t)]$. Here, $|\phi_0^R(\boldsymbol{\lambda}_{\text{tar}} - \Delta\lambda \mathbf{e}_\mu)\rangle$ is the right ground state of $H(\boldsymbol{\lambda}_{\text{tar}} - \Delta\lambda \mathbf{e}_\mu)$, and the parameters evolve along the μ-direction follows [92]:

$$\boldsymbol{\lambda}(t) = \boldsymbol{\lambda}_{\text{tar}} - \Delta\lambda \mathbf{e}_\mu + \frac{v^2 t^2}{4\Delta\lambda}\mathbf{e}_\mu, \quad t \in [0, t_f], \quad (5)$$

where $t_f = 2\Delta\lambda/v$, $\Delta\lambda$ is a preset constant, and $\mathbf{e}_\mu$ denotes the unit vector along the μ-th parameter direction. This ramping profile guarantees that the initial evolution is adiabatic, suppressing oscillations induced by the initial state [92]. The final speed v and the preset value $\Delta\lambda$ are calibrated to satisfy adiabatic perturbation theory [81–84].

Additionally, we prepare the time-evolved states $|\psi_\mu'(\boldsymbol{\lambda}_{\text{tar}}, t)\rangle$ and $|\psi_\mu''(\boldsymbol{\lambda}_{\text{tar}}, t)\rangle$ by evolving the left ground state $|\phi_0^L(\boldsymbol{\lambda}_{\text{tar}} - \Delta\lambda \mathbf{e}_\mu)\rangle$ under $H^\dagger[\boldsymbol{\lambda}(t)]$ and $-H^\dagger[\boldsymbol{\lambda}(t)]$, respectively. The parameter evolution $\boldsymbol{\lambda}(t)$ is identical to Eq. (5).

Scheme 1: QGT measurement via energy fluctuations. The generalized expectation value of the energy fluctuation operator $\Delta^2 H \equiv (H - \langle H \rangle)^2 \approx (H - E_0)^2$ with respect to the pair of time-evolved states $|\psi_\mu'(\boldsymbol{\lambda}_{\text{tar}}, t)\rangle$ and $|\psi_\nu(\boldsymbol{\lambda}_{\text{tar}}, t)\rangle$ is

$$\frac{\langle \psi_\mu'(\boldsymbol{\lambda}_{\text{tar}}, t)|(H - E_0)^2|\psi_\nu(\boldsymbol{\lambda}_{\text{tar}}, t)\rangle}{\langle \psi_\mu'(\boldsymbol{\lambda}_{\text{tar}}, t)|\psi_\nu(\boldsymbol{\lambda}_{\text{tar}}, t)\rangle} \approx v^2 Q_{\mu\nu}^0(\boldsymbol{\lambda}_{\text{tar}}). \quad (6)$$

Dividing this complex expectation value by v^2 directly yields both the real and imaginary parts of the target QGT component $Q_{\mu\nu}^0(\boldsymbol{\lambda}_{\text{tar}})$. $(H - E_0)^2$ is called the square of the absolute Hamiltonian, which differs from energy fluctuation by high-order negligible terms [48].

Scheme 2: QGT measurement via generalized forces. The imaginary part of the QGT is measured from the generalized expectation value of the generalized force operator $f_\mu \equiv -\partial_\mu H$ with respect to the pair of time-evolved states $|\psi_\nu'(\boldsymbol{\lambda}_{\text{tar}}, t)\rangle$ and $|\psi_\nu(\boldsymbol{\lambda}_{\text{tar}}, t)\rangle$, i.e.,

$$\frac{\langle \psi_\nu'(\boldsymbol{\lambda}_{\text{tar}}, t)|(-\partial_\mu H)|\psi_\nu(\boldsymbol{\lambda}_{\text{tar}}, t)\rangle}{\langle \psi_\nu'(\boldsymbol{\lambda}_{\text{tar}}, t)|\psi_\nu(\boldsymbol{\lambda}_{\text{tar}}, t)\rangle}$$
$$\approx \langle f_\mu(\boldsymbol{\lambda}_{\text{tar}})\rangle - 2v\text{Im}\left[Q_{\mu\nu}^0(\boldsymbol{\lambda}_{\text{tar}})\right] \quad (7)$$
$$= \langle f_\mu(\boldsymbol{\lambda}_{\text{tar}})\rangle + vF_{\mu\nu}^0(\boldsymbol{\lambda}_{\text{tar}}). \quad (8)$$

where the constant term $\langle f_\mu(\boldsymbol{\lambda}_{\text{tar}})\rangle$ is defined as the generalized expectation value of the generalized force operator with respect to the instantaneous eigenstates $|\phi_0^L(\boldsymbol{\lambda}_{\text{tar}})\rangle$ and $|\phi_0^R(\boldsymbol{\lambda}_{\text{tar}})\rangle$ at the target point $\boldsymbol{\lambda}_{\text{tar}}$, i.e.,

$$\langle f_\mu(\boldsymbol{\lambda}_{\text{tar}})\rangle = \frac{\langle \phi_0^L(\boldsymbol{\lambda}_{\text{tar}})|(-\partial_\mu H)|\phi_0^R(\boldsymbol{\lambda}_{\text{tar}})\rangle}{\langle \phi_0^L(\boldsymbol{\lambda}_{\text{tar}})|\phi_0^R(\boldsymbol{\lambda}_{\text{tar}})\rangle}. \quad (9)$$

After subtracting the constant, the coefficient of v gives the target Berry curvature $F_{\mu\nu}^0(\boldsymbol{\lambda}_{\text{tar}}) = -2\text{Im}[Q_{\mu\nu}^0(\boldsymbol{\lambda}_{\text{tar}})] = 2\text{Im}[Q_{\nu\mu}^0(\boldsymbol{\lambda}_{\text{tar}})]$.

By substituting another pair of time-evolved states, $|\psi_\nu''(\boldsymbol{\lambda}_{\text{tar}}, t)\rangle$ and $|\psi_\nu(\boldsymbol{\lambda}_{\text{tar}}, t)\rangle$, to construct the generalized expectation value of the generalized force operator, we obtain the real part of the QGT

$$\frac{\langle \psi_\nu''(\boldsymbol{\lambda}_{\text{tar}}, t)|(-\partial_\mu H)|\psi_\nu(\boldsymbol{\lambda}_{\text{tar}}, t)\rangle}{\langle \psi_\nu''(\boldsymbol{\lambda}_{\text{tar}}, t)|\psi_\nu(\boldsymbol{\lambda}_{\text{tar}}, t)\rangle}$$
$$\approx \langle f_\mu(\boldsymbol{\lambda}_{\text{tar}})\rangle + 2iv\text{Re}\left[Q_{\mu\nu}^0(\boldsymbol{\lambda}_{\text{tar}})\right] \quad (10)$$
$$= \langle f_\mu(\boldsymbol{\lambda}_{\text{tar}})\rangle + i2vg_{\mu\nu}^0(\boldsymbol{\lambda}_{\text{tar}}). \quad (11)$$

where $|\psi_\nu''(\boldsymbol{\lambda}_{\text{tar}}, t)\rangle$ evolves under $-H^\dagger[\boldsymbol{\lambda}(t)]$. The imaginary part of this generalized expectation value, divided by $2v$ after subtracting the constant, yields the target quantum metric $g_{\mu\nu}^0(\boldsymbol{\lambda}_{\text{tar}}) = \text{Re}[Q_{\mu\nu}^0(\boldsymbol{\lambda}_{\text{tar}})]$.

IV. EXAMPLES

We verify both schemes using two distinct 2-band models, constructed from q-deformed Pauli matrices [65, 66, 93]:

$$\tilde{\sigma}_x = \begin{bmatrix} 0 & a \\ b & 0 \end{bmatrix}, \ \tilde{\sigma}_y = \begin{bmatrix} 0 & -ia \\ ib & 0 \end{bmatrix}, \ \tilde{\sigma}_z = \begin{bmatrix} q^{-1} & 0 \\ 0 & -q \end{bmatrix}, \quad (12)$$

where $a = \sqrt{(1 + q^2)/2}$, $b = \sqrt{(1 + q^{-2})/2}$, and $q > 0$. These systems are pseudo-Hermitian, satisfying $H^\dagger = \eta H \eta^{-1}$ with $\eta = \text{diag}(q^{-1/2}, q^{1/2})$, and reduce to Hermitian at $q = 1$. Their Hamiltonian

$$H = \mathbf{d} \cdot \tilde{\boldsymbol{\sigma}} = d_x \tilde{\sigma}_x + d_y \tilde{\sigma}_y + d_z \tilde{\sigma}_z, \quad (13)$$

has real eigenvalues $E_\pm = d d_z \pm \sqrt{ab(d_x^2 + d_y^2) + c^2 d_z^2}$ with $c = (1 + q^2)/(2q)$ and $d = (1 - q^2)/(2q)$. Here, $\mathbf{d}$ represents the Bloch vector which varies across different models. The generalized force operator reduces to $f_\mu = -\partial_\mu H = -(\partial_\mu \mathbf{d}) \cdot \tilde{\boldsymbol{\sigma}}$ with the partial derivative of the Bloch vector. Throughout the benchmark tests, we fix $q = 3$.

A. Model I with nontrivial topology

The first model is defined by the Bloch vector $\mathbf{d}(\theta, \phi) = \frac{1}{2}(\Omega_1 \sin\theta \cos\phi, \Omega_1 \sin\theta \sin\phi, \Delta_1 \cos\theta + \Delta_2)$, whose Hermitian counterpart maps onto the Haldane model [32, 94]. This model exhibits nontrivial Chern numbers $C = \frac{1}{2\pi}\int_S F_{\theta\phi} \ \mathrm{d}S = \int_0^\pi F_{\theta\phi} \ d\theta$, defined by the Berry curvature $F_{\theta\phi} = 2\text{Im}[Q_{\phi\theta}]$, in specific parameter regimes. Notably, its off-diagonal quantum metric vanishes across the entire parameter space, i.e., $\text{Re}[Q_{\phi\theta}] = \text{Re}[Q_{\theta\phi}] = 0$.

To measure the QGT at target parameters $(\theta_{\text{tar}}, \phi_{\text{tar}})$, we implement the following steps with $\Delta\theta = \pi/2$, $v = 1$, and $t_f = \pi$. The time-evolved states $|\psi_\theta[(\theta_{\text{tar}}, \phi_{\text{tar}}), t]\rangle$ and $|\psi_\phi[(\theta_{\text{tar}}, \phi_{\text{tar}}), t]\rangle$ are generated from initial right eigenstates $|\phi_0^R(\theta_{\text{tar}} - \frac{\pi}{2}, \phi_{\text{tar}})\rangle$ and $|\phi_0^R(\theta_{\text{tar}}, \phi_{\text{tar}} - \frac{\pi}{2})\rangle$, respectively, by time evolution under $H[\theta(t), \phi(t)]$ with distinct time-dependent parameters. For parameters drift along the θ-direction or ϕ-direction, we set $\theta(t)$ and $\phi(t)$ evolve as follows:

$$\theta\text{-direction}: \quad \theta(t) = \theta_{\text{tar}} - \frac{\pi}{2} + \frac{t^2}{2\pi}, \quad \phi(t) = 0 \quad (14)$$

$$\phi\text{-direction}: \quad \theta(t) = \theta_{\text{tar}}, \quad \phi(t) = -\frac{\pi}{2} + \frac{t^2}{2\pi}. \quad (15)$$

States $|\psi_{\theta,\phi}'[(\theta_{\text{tar}}, \phi_{\text{tar}}), t]\rangle$ and $|\psi_{\theta,\phi}''[(\theta_{\text{tar}}, \phi_{\text{tar}}), t]\rangle$ evolve under $H^\dagger[\theta(t), \phi(t)]$ and $-H^\dagger[\theta(t), \phi(t)]$, respectively, from initial left eigenstates. After preparing these states, the QGT can be measured through the generalized expectation values of either the energy fluctuation operator (Eq. (6)) or the generalized force operators (Eqs. (7) and (11)) with the corresponding prepared states. In this model, the generalized force operators are defined as

$$f_\theta = -\frac{1}{2}(\Omega_1 \cos\theta \cos\phi, \Omega_1 \cos\theta \sin\phi, -\Delta_1 \sin\theta) \cdot \tilde{\boldsymbol{\sigma}},$$
$$f_\phi = -\frac{1}{2}(-\Omega_1 \sin\theta \sin\phi, \Omega_1 \sin\theta \cos\phi, 0) \cdot \tilde{\boldsymbol{\sigma}}. \quad (16)$$
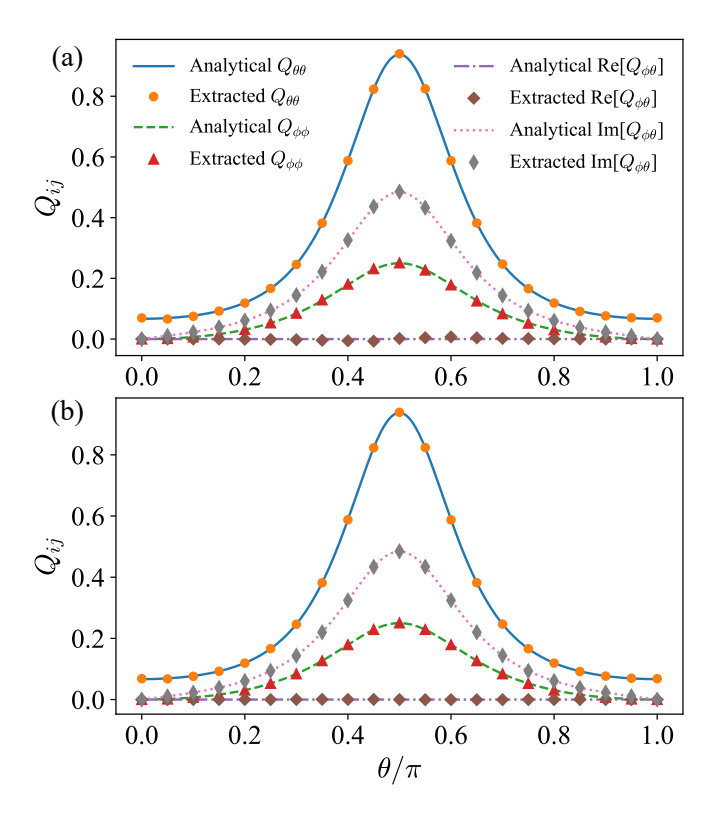
FIG. 1. QGT components for Model I, extracted via (a) energy fluctuation and (b) generalized force schemes. Analytical results (lines) and numerical data (markers) are shown for $Q_{\theta\theta}$ (solid/circles), $Q_{\phi\phi}$ (dashed/triangles), $\mathrm{Re}[Q_{\phi\theta}]$ (dashdotted/diamonds), and $\mathrm{Im}[Q_{\phi\theta}]$ (dotted/squares). Parameters are fixed at $\Omega_1/2\pi = 10$, $\Delta_1/2\pi = 15$, $\Delta_2 = 0$ and $\phi = 0$.

As a demonstration, we extract the QGT components $Q_{\theta\theta}$, $Q_{\phi\phi}$, $\mathrm{Re}[Q_{\phi\theta}]$, and $\mathrm{Im}[Q_{\phi\theta}]$ at $\Omega_1/2\pi = 10$, $\Delta_1/2\pi = 15$, $\Delta_2 = 0$, $\phi_{\mathrm{tar}} = 0$, sampling θ_{tar} at $N = 21$ points over $[0, \pi]$. Fig. 1 shows excellent agreement between the numerical extracted data of both schemes and analytical predictions. The generalized force scheme achieves higher accuracy for the off-diagonal metric $\mathrm{Re}[Q_{\phi\theta}]$.

For fixed parameters $\Omega_1/2\pi = 10$ and $\Delta_1/2\pi = 15$, a topological transition occurs at $\Delta_2/\Delta_1 = 1$. Fig. 2 compares Chern numbers calculated from Berry curvatures extracted via both schemes across $\Delta_2/2\pi \in [0, 30]$ ($\Delta_2/\Delta_1 \in [0, 2]$). For each Δ_2, we integrate $F_{\theta\phi}$ over $\theta \in [0, \pi]$ using $N = 21$ discrete points. Both methods agree with theory except near the critical point $\Delta_2/\Delta_1 = 1$, where numerical accuracy improves with increased sampling density.

B. Model II with a nonvanishing off-diagonal quantum metric

The Bloch vector for the second model is $\mathbf{d}(x, y) = B[\sin(x + y)\cos(xy), \sin(x + y)\sin(xy), \cos(x + y)]$ [48], engineered to exhibit nonvanishing off-diagonal quantum
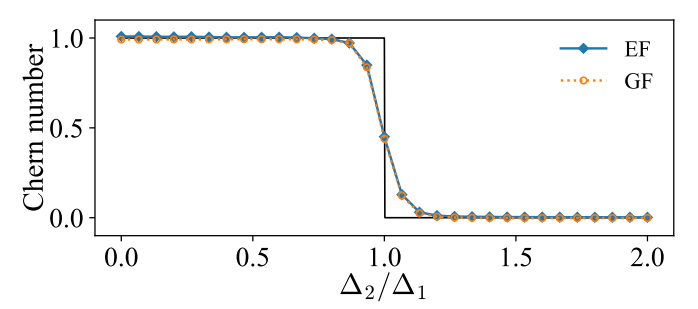

FIG. 2. Chern number Phase diagram for Model I. Data from energy fluctuation (diamonds) and generalized force (circles) schemes are compared with analytical predictions (solid line). Parameters are fixed at $\Omega_1/2\pi = 10$ and $\Delta_1/2\pi = 15$, while $\Delta_2/2\pi$ is scanned from 0 to 30 (corresponding to Δ_2/Δ_1 from 0 to 2).

metric component, i.e., $\mathrm{Re}[Q_{\phi\theta}] = \mathrm{Re}[Q_{\theta\phi}] \neq 0$.

Using identical scheme parameters ($\Delta x = \pi/2$, $v = 1$, $t_f = \pi$), we implement parameter drifts with $x(t) = x_{\mathrm{tar}} - \frac{\pi}{2} + \frac{t^2}{2\pi}$ and $y(t) = y_{\mathrm{tar}}$ for the x direction, while for the y direction, we set $x(t) = x_{\mathrm{tar}}$, $y(t) = y_{\mathrm{tar}} - \frac{\pi}{2} + \frac{t^2}{2\pi}$. Target states $|\psi_{x,y}[(x_{\mathrm{tar}}, y_{\mathrm{tar}}), t]\rangle$ are prepared following the same procedure as in Sec. IV A. The corresponding target states $|\psi'_{x,y}[(x_{\mathrm{tar}}, y_{\mathrm{tar}}), t]\rangle$, $|\psi''_{x,y}[(x_{\mathrm{tar}}, y_{\mathrm{tar}}), t]\rangle$ are generated by the similar way.

At $B/2\pi = 15$ and $y_{\mathrm{tar}} = \pi/2$, with x_{tar} sampled at $N = 21$ points over $[-2\pi, 2\pi]$, Fig. 3 demonstrates highfidelity extraction of Q_{xx}, Q_{yy}, $\mathrm{Re}[Q_{yx}]$, and $\mathrm{Im}[Q_{yx}]$ for both protocols.

V. EXPERIMENTAL IMPLEMENTATION

The schemes for extracting the QGT in pseudo-Hermitian systems with real spectra can be implemented on current quantum devices, such as nitrogen vacancy (NV) centers [95–98] and superconducting qubits [99], through three sequential steps. Nonunitary evolutions in Steps 1 and 2 are embedded in larger unitary evolutions using the dilation method [95–98, 100].

Step 1: Ground State Preparation. We initialize the qubit system in a computational basis state, such as $[0, 1]^T$ for a single qubit, corresponding to the ground state of $H(\boldsymbol{\lambda})$ at reference parameters (e.g., $(\theta, \phi) = (0, 0)$ for the Model I or $(x, y) = (0, 0)$ for the Model II). Next, we adiabatically ramp the parameters $\boldsymbol{\lambda}$ to the target point with a preset value along the μ-th direction, i.e., $\boldsymbol{\lambda}_{\mathrm{tar}} - \Delta\lambda\mathbf{e}_\mu$, to prepare the right and left ground states of $H(\boldsymbol{\lambda}_{\mathrm{tar}} - \Delta\lambda\mathbf{e}_\mu)$, denoted $|\phi_0^R(\boldsymbol{\lambda}_{\mathrm{tar}} - \Delta\lambda\mathbf{e}_\mu)\rangle$ and $|\phi_0^L(\boldsymbol{\lambda}_{\mathrm{tar}} - \Delta\lambda\mathbf{e}_\mu)\rangle$. The adiabatic condition requires the ramping speed v to satisfy $|v| \ll \min_{\boldsymbol{\lambda}} |\Delta E| / |\langle\phi_1^L|\partial_\mu H|\phi_0^R\rangle|$, where ΔE denotes the energy gap between the ground state and the first excited state.

Step 2: State Evolution. We evolve the prepared right ground state $|\phi_0^R(\boldsymbol{\lambda}_{\mathrm{tar}} - \Delta\lambda\mathbf{e}_\mu)\rangle$ under the timedependent Hamiltonian $H[\boldsymbol{\lambda}(t)]$ to obtain the target
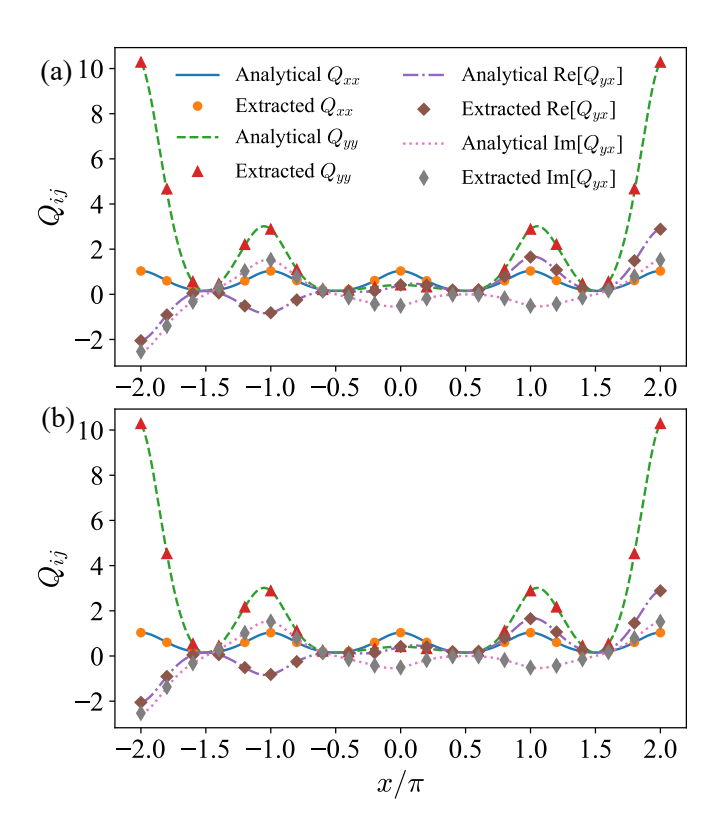
FIG. 3. QGT components for Model II, extracted via (a) energy fluctuation and (b) generalized force schemes. The line and marker styles match those in Fig. 1, with the only difference being in the corresponding subscript. Parameters are fixed at $B/2\pi = 15$ and $y = \pi/2$.

state $|\psi_\mu(\boldsymbol{\lambda}_{\text{tar}}, t)\rangle$, while evolving the left ground state $|\phi_0^L(\boldsymbol{\lambda}_{\text{tar}} - \Delta\lambda\mathbf{e}_\mu)\rangle$ under $H^\dagger[\boldsymbol{\lambda}(t)]$ to obtain $|\psi'_\mu(\boldsymbol{\lambda}_{\text{tar}}, t)\rangle$ and under $-H^\dagger[\boldsymbol{\lambda}(t)]$ to obtain $|\psi''_\mu(\boldsymbol{\lambda}_{\text{tar}}, t)\rangle$, with the parameter trajectory $\boldsymbol{\lambda}(t)$ following Eq. (5) in all cases.

Step 3: Generalized Expectation Value Measurement. The generalized expectation value can be measured using the quantum circuit proposed in Refs. [85–87] (See Appendix B for details). For the energy fluctuation scheme, the input states are $|\psi_1\rangle = |\psi'_\mu(\boldsymbol{\lambda}_{\text{tar}}, t)\rangle$ and $|\psi_2\rangle = |\psi_\nu(\boldsymbol{\lambda}_{\text{tar}}, t)\rangle$ with operator $A = \Delta^2 H = (H - \langle H\rangle)^2$. For the generalized force scheme with $A = f_\mu = -\partial_\mu H$, the Berry curvature is measured using $|\psi_1\rangle = |\psi'_\nu(\boldsymbol{\lambda}_{\text{tar}}, t)\rangle$ and $|\psi_2\rangle = |\psi_\nu(\boldsymbol{\lambda}_{\text{tar}}, t)\rangle$, while the quantum metric is measured using $|\psi_1\rangle = |\psi''_\mu(\boldsymbol{\lambda}_{\text{tar}}, t)\rangle$ and $|\psi_2\rangle = |\psi_\nu(\boldsymbol{\lambda}_{\text{tar}}, t)\rangle$. The constant in Eq. (9) is obtained from the ground-state generalized expectation value at $\boldsymbol{\lambda}_{\text{tar}}$ using $|\psi_1\rangle = |\phi_0^L(\boldsymbol{\lambda}_{\text{tar}})\rangle$ and $|\psi_2\rangle = |\phi_0^R(\boldsymbol{\lambda}_{\text{tar}})\rangle$, which can be prepared by adiabatically ramping $\boldsymbol{\lambda}$ from the reference parameters to $\boldsymbol{\lambda}_{\text{tar}}$.

VI. CONCLUSION AND DISCUSSION

We establish two independent schemes for directly measuring all components of the QGT, defined using both left and right eigenstates, in pseudo-Hermitian systems with real spectra. The first scheme employs the energy fluctuation operator $\Delta^2 H \equiv (H - \langle H\rangle)^2$, while the second utilizes the generalized force operator $f_\mu = -\partial_\mu H$, with each providing self-contained pathways to determine the complete QGT. Numerical verification on two q-deformed models (Figs. 1 and 3) demonstrates high-fidelity agreement with analytical predictions for both schemes. Furthermore, the Chern number phase diagram of the first model (Fig. 2) confirms that both schemes can build up topological invariants, a task previously achievable only through generalized force schemes in Hermitian systems.

From a quantum measurement perspective, the generalized force operator requires fewer measurements than the energy fluctuation operator due to vanishing partial derivatives for certain measurement bases, such as the σ_z-component-free f_ϕ operator in Eqs. (16). Consequently, the generalized force scheme provides superior measurement efficiency that scales with system dimension. Notably, both schemes remain applicable to Hermitian systems, establishing a unified experimental framework for directly measuring QGT across Hermitian and non-Hermitian regimes with nonadiabatic response [101]. We expect that this framework can be extended to directly measure other physical quantities in LR formalism via dynamic processes.

Appendix A: Adiabatic Perturbation Theory for Pseudo-Hermitian Systems

In this Appendix, we overview the adiabatic perturbation theory for pseudo-Hermitian systems with real spectra [81–84].

Adiabatic perturbation theory provides a framework for analyzing time evolution under monotonic parameter drifts. We examine the dynamics of a quantum state $|\psi[\lambda(t)]\rangle$ evolving under a time-dependent pseudo-Hermitian Hamiltonian $H[\lambda(t)]$ with real spectra, where $\lambda(t)$ denotes a monotonically and slowly varying parameter with nonzero velocity $v_\lambda(t) \equiv \dot\lambda(t) \neq 0$. The reality of the energy spectra ensures that the dynamical phases $\Theta_n(t) = \int_0^t dt' E_n[\lambda(t')]$ remain strictly real-valued. Concurrently, the pseudo-Hermitian condition $H^\dagger = \eta H \eta^{-1}$ guarantees that the geometric phases $\Phi_n(t) = -i\int_0^t dt' \langle\phi_n^L[\lambda(t')]|\partial_{t'}\phi_n^R[\lambda(t')]\rangle$ are also real.

By adapting adiabatic perturbation theory to pseudo-Hermitian systems, we obtain the state evolving from the instantaneous right ground state of $H[\lambda(0)]$ at the initial time, i.e., $|\phi_0^R[\lambda(0)]\rangle$, and expand it in terms of the instantaneous right eigenstates $|\phi_m^R[\lambda(t)]\rangle$ of $H[\lambda(t)]$:

$$|\psi[\lambda(t)]\rangle = |\phi_0^R[\lambda(t)]\rangle + \sum_{m\neq 0} a_m(t)|\phi_m^R[\lambda(t)]\rangle + \mathcal{O}(v_\lambda^2),$$
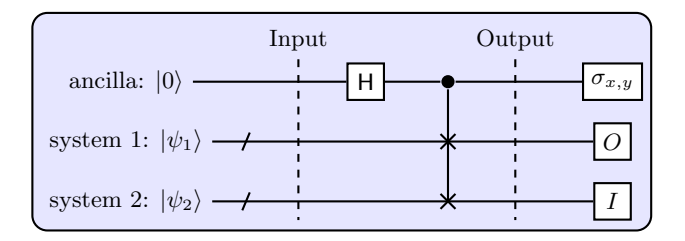(A1)

FIG. 4. Quantum circuit for measuring the generalized expectation value $\frac{\langle\psi_1|O|\psi_2\rangle}{\langle\psi_1|\psi_2\rangle}$ via a controlled SWAP operation. The ancilla qubit (top line) controls a SWAP operation between two n-qubit registers storing arbitrary states $|\psi_1\rangle$ and $|\psi_2\rangle$. Measurement of σ_x (σ_y) on the ancilla yields the real (imaginary) part of $\langle\psi_1|O|\psi_2\rangle\langle\psi_2|\psi_1\rangle$, which corresponds to the numerator of the generalized expectation value. The denominator $|\langle\psi_1|\psi_2\rangle|^2$ is obtained by setting O as the identity matrix I and measuring σ_x on the ancilla.

where the expansion coefficients $a_m(t)$ are given by

$$a_m(t) = iv_\lambda(t)\frac{\langle\phi_m^L[\lambda(t)]|\partial_\lambda\phi_0^R[\lambda(t)]\rangle}{E_m[\lambda(t)] - E_0[\lambda(t)]}. \qquad (A2)$$

Appendix B: Quantum Circuit for Measuring Generalized Expectation Values

In this Appendix, we briefly introduce the quantum circuit for measuring the generalized expectation value in Ref. [85].

We restrict our consideration to measuring $\frac{\langle\psi_1|O|\psi_2\rangle}{\langle\psi_1|\psi_2\rangle}$, where O is a experimentally accessible Hermitian observable, because any operator A can be expressed as a linear combination of Hermitian operators via the decomposition $A = \left(\frac{A+A^\dagger}{2}\right) + i\left(\frac{A-A^\dagger}{2i}\right)$.

The input state of the quantum circuit comprises an ancilla qubit in $|0\rangle$ and two n-qubit registers initialized

to arbitrary states $|\psi_1\rangle$ and $|\psi_2\rangle$, expressed as:

$$|\Psi_{\text{input}}\rangle = |0\rangle \otimes |\psi_1\rangle \otimes |\psi_2\rangle. \qquad (B1)$$

The circuit executes sequential operations beginning with a Hadamard gate H applied to the ancilla qubit, followed by a controlled SWAP operation acting on the two n-qubit registers with the ancilla as control. These operations generate the output state

$$|\Psi_{\text{output}}\rangle = \frac{1}{\sqrt{2}}\left(|0\rangle \otimes |\psi_1\rangle \otimes |\psi_2\rangle + |1\rangle \otimes |\psi_2\rangle \otimes |\psi_1\rangle\right). \qquad (B2)$$

The expectation value of $\sigma_x \otimes O \otimes I$ or $\sigma_y \otimes O \otimes I$ with respect to $|\Psi_{\text{output}}\rangle$ gives the real or imaginary part of $\langle\psi_1|O|\psi_2\rangle\langle\psi_2|\psi_1\rangle$, respectively, i.e.,

$$\langle\Psi_{\text{output}}|\sigma_{x,y} \otimes O \otimes I|\Psi_{\text{output}}\rangle = \text{Re}, \text{Im}\left[\langle\psi_1|O|\psi_2\rangle\langle\psi_2|\psi_1\rangle\right] \qquad (B3)$$

where O denotes any experimentally accessible Hermitian operator. Setting O as the identity operator I, Eq. (B3) simplifies to

$$\langle\Psi_{\text{output}}|\sigma_x \otimes I \otimes I|\Psi_{\text{output}}\rangle = |\langle\psi_1|\psi_2\rangle|^2. \qquad (B4)$$

The real and imaginary parts of the generalized expectation value $\frac{\langle\psi_1|O|\psi_2\rangle}{\langle\psi_1|\psi_2\rangle}$ are obtained from the quotients

$$\text{Re}, \text{Im}\left[\frac{\langle\psi_1|O|\psi_2\rangle}{\langle\psi_1|\psi_2\rangle}\right] = \frac{\langle\Psi_{\text{output}}|\sigma_{x,y} \otimes O \otimes I|\Psi_{\text{output}}\rangle}{\langle\Psi_{\text{output}}|\sigma_x \otimes I \otimes I|\Psi_{\text{output}}\rangle}. \qquad (B5)$$

ACKNOWLEDGMENTS

[1] P. Törmä, S. Peotta, and B. A. Bernevig, Nature Reviews Physics **4**, 528 (2022).

[2] P. Törmä, Phys. Rev. Lett. **131**, 240001 (2023).

[3] S.-L. Zhu, International Journal of Modern Physics B **22**, 561 (2008).

[4] J. P. Provost and G. Vallee, Communications in Mathematical Physics **76**, 289 (1980).

[5] S. L. Braunstein and C. M. Caves, Phys. Rev. Lett. **72**, 3439 (1994).

[6] S. Peotta and P. Törmä, Nature Communications **6**, 8944 (2015).

[7] A. Julku, S. Peotta, T. I. Vanhala, D.-H. Kim, and P. Törmä, Phys. Rev. Lett. **117**, 045303 (2016).

[8] L. Liang, T. I. Vanhala, S. Peotta, T. Siro, A. Harju, and P. Törmä, Phys. Rev. B **95**, 024515 (2017).

[9] Y. Gao, S. A. Yang, and Q. Niu, Phys. Rev. B **91**, 214405 (2015).

[10] F. Piéchon, A. Raoux, J.-N. Fuchs, and G. Montambaux, Phys. Rev. B **94**, 134423 (2016).

[11] Z. Z. Du, H.-Z. Lu, and X. C. Xie, Nature Reviews Physics **3**, 744 (2021).

[12] A. Gao, Y.-F. Liu, J.-X. Qiu, B. Ghosh, T. V. Trevisan, Y. Onishi, C. Hu, T. Qian, H.-J. Tien, S.-W. Chen, M. Huang, D. Bérubé, H. Li, C. Tzschaschel, T. Dinh, Z. Sun, S.-C. Ho, S.-W. Lien, B. Singh, K. Watanabe, T. Taniguchi, D. C. Bell, H. Lin, T.-R. Chang, C. R.

Du, A. Bansil, L. Fu, N. Ni, P. P. Orth, Q. Ma, and S.-Y. Xu, Science **381**, 181 (2023).

[13] N. Wang, D. Kaplan, Z. Zhang, T. Holder, N. Cao, A. Wang, X. Zhou, F. Zhou, Z. Jiang, C. Zhang, S. Ru, H. Cai, K. Watanabe, T. Taniguchi, B. Yan, and W. Gao, Nature **621**, 487 (2023).

[14] D. Xiao, M.-C. Chang, and Q. Niu, Rev. Mod. Phys. **82**, 1959 (2010).

[15] B. Simon, Phys. Rev. Lett. **51**, 2167 (1983).

[16] M. V. Berry, Proceedings of the Royal Society of London. A. Mathematical and Physical Sciences **392**, 45 (1984).

[17] D. J. Thouless, M. Kohmoto, M. P. Nightingale, and M. den Nijs, Phys. Rev. Lett. **49**, 405 (1982).

[18] M. Z. Hasan and C. L. Kane, Rev. Mod. Phys. **82**, 3045 (2010).

[19] X.-L. Qi and S.-C. Zhang, Rev. Mod. Phys. **83**, 1057 (2011).

[20] N. P. Armitage, E. J. Mele, and A. Vishwanath, Rev. Mod. Phys. **90**, 015001 (2018).

[21] S.-L. Zhu, H. Fu, C.-J. Wu, S.-C. Zhang, and L.-M. Duan, Phys. Rev. Lett. **97**, 240401 (2006).

[22] D.-W. Zhang, Y.-Q. Zhu, Y. X. Zhao, H. Yan, and S.-L. Zhu, Advances in Physics **67**, 253 (2018).

[23] A. C. M. Carollo and J. K. Pachos, Phys. Rev. Lett. **95**, 157203 (2005).

[24] S.-L. Zhu, Phys. Rev. Lett. **96**, 077206 (2006).

[25] L. Campos Venuti and P. Zanardi, Phys. Rev. Lett. **99**, 095701 (2007).

[26] S.-J. Gu, H.-M. Kwok, W.-Q. Ning, and H.-Q. Lin, Phys. Rev. B **77**, 245109 (2008).

[27] Y.-Q. Ma, S. Chen, H. Fan, and W.-M. Liu, Phys. Rev. B **81**, 245129 (2010).

[28] H.-T. Ding, C.-X. Zhang, J.-X. Liu, J.-T. Wang, D.-W. Zhang, and S.-L. Zhu, Phys. Rev. A **109**, 043305 (2024).

[29] X.-Y. Hou, Z. Zhou, X. Wang, H. Guo, and C.-C. Chien, Phys. Rev. B **110**, 035144 (2024).

[30] Z. Zhou, X.-Y. Hou, X. Wang, J.-C. Tang, H. Guo, and C.-C. Chien, Phys. Rev. B **110**, 035404 (2024).

[31] Q. Wang, B. Wang, J. Wang, and L. Zhang, Chinese Physics Letters **42**, 070603 (2025).

[32] M. D. Schroer, M. H. Kolodrubetz, W. F. Kindel, M. Sandberg, J. Gao, M. R. Vissers, D. P. Pappas, A. Polkovnikov, and K. W. Lehnert, Phys. Rev. Lett. **113**, 050402 (2014).

[33] P. Roushan, C. Neill, Y. Chen, M. Kolodrubetz, C. Quintana, N. Leung, M. Fang, R. Barends, B. Campbell, Z. Chen, B. Chiaro, A. Dunsworth, E. Jeffrey, J. Kelly, A. Megrant, J. Mutus, P. J. J. O'Malley, D. Sank, A. Vainsencher, J. Wenner, T. White, A. Polkovnikov, A. N. Cleland, and J. M. Martinis, Nature **515**, 241 (2014).

[34] X. Tan, D.-W. Zhang, Q. Liu, G. Xue, H.-F. Yu, Y.-Q. Zhu, H. Yan, S.-L. Zhu, and Y. Yu, Phys. Rev. Lett. **120**, 130503 (2018).

[35] X. Tan, Y. X. Zhao, Q. Liu, G. Xue, H.-F. Yu, Z. D. Wang, and Y. Yu, Phys. Rev. Lett. **122**, 010501 (2019).

[36] X. Tan, D.-W. Zhang, Z. Yang, J. Chu, Y.-Q. Zhu, D. Li, X. Yang, S. Song, Z. Han, Z. Li, Y. Dong, H.-F. Yu, H. Yan, S.-L. Zhu, and Y. Yu, Phys. Rev. Lett. **122**, 210401 (2019).

[37] X. Tan, D.-W. Zhang, W. Zheng, X. Yang, S. Song, Z. Han, Y. Dong, Z. Wang, D. Lan, H. Yan, S.-L. Zhu,

and Y. Yu, Phys. Rev. Lett. **126**, 017702 (2021).

[38] T. Chen, H.-T. Ding, R. Shen, S.-L. Zhu, and J. Gong, Phys. Rev. B **110**, 205402 (2024).

[39] D. T. Tran, A. Dauphin, A. G. Grushin, P. Zoller, and N. Goldman, Science Advances **3**, e1701207 (2017).

[40] T. Ozawa and N. Goldman, Phys. Rev. B **97**, 201117 (2018).

[41] L. Asteria, D. T. Tran, T. Ozawa, M. Tarnowski, B. S. Rem, N. Fläschner, K. Sengstock, N. Goldman, and C. Weitenberg, Nature Physics **15**, 449 (2019).

[42] Q.-X. Lv, Y.-X. Du, Z.-T. Liang, H.-Z. Liu, J.-H. Liang, L.-Q. Chen, L.-M. Zhou, S.-C. Zhang, D.-W. Zhang, B.-Q. Ai, H. Yan, and S.-L. Zhu, Phys. Rev. Lett. **127**, 136802 (2021).

[43] H.-T. Ding, Y.-Q. Zhu, P. He, Y.-G. Liu, J.-T. Wang, D.-W. Zhang, and S.-L. Zhu, Phys. Rev. A **105**, 012210 (2022).

[44] C.-R. Yi, J. Yu, H. Yuan, R.-H. Jiao, Y.-M. Yang, X. Jiang, J.-Y. Zhang, S. Chen, and J.-W. Pan, Phys. Rev. Res. **5**, L032016 (2023).

[45] S.-L. Zhu, B. Wang, and L.-M. Duan, Phys. Rev. Lett. **98**, 260402 (2007).

[46] M. Yu, P. Yang, M. Gong, Q. Cao, Q. Lu, H. Liu, S. Zhang, M. B. Plenio, F. Jelezko, T. Ozawa, N. Goldman, and J. Cai, National Science Review **7**, 254 (2019).

[47] M. Chen, C. Li, G. Palumbo, Y.-Q. Zhu, N. Goldman, and P. Cappellaro, Science **375**, 1017 (2022).

[48] X. Zhang, X.-M. Lu, J. Liu, W. Ding, and X. Wang, Phys. Rev. A **107**, 012414 (2023).

[49] A. Gianfrate, O. Bleu, L. Dominici, V. Ardizzone, M. De Giorgi, D. Ballarini, G. Lerario, K. W. West, L. N. Pfeiffer, D. D. Solnyshkov, D. Sanvitto, and G. Malpuech, Nature **578**, 381 (2020).

[50] S. Kim, Y. Chung, Y. Qian, S. Park, C. Jozwiak, E. Rotenberg, A. Bostwick, K. S. Kim, and B.-J. Yang, Science **388**, 1050 (2025).

[51] A. Ghatak and T. Das, Journal of Physics: Condensed Matter **31**, 263001 (2019).

[52] Y. Ashida, Z. Gong, and M. Ueda, Advances in Physics **69**, 249 (2020).

[53] E. J. Bergholtz, J. C. Budich, and F. K. Kunst, Rev. Mod. Phys. **93**, 015005 (2021).

[54] D. D. Solnyshkov, C. Leblanc, L. Bessonart, A. Nalitov, J. Ren, Q. Liao, F. Li, and G. Malpuech, Phys. Rev. B **103**, 125302 (2021).

[55] B. Alon, R. Ilan, and M. Goldstein, Phys. Rev. B **110**, 245103 (2024).

[56] J. Cuerda, J. M. Taskinen, N. Källman, L. Grabitz, and P. Törmä, Phys. Rev. B **109**, 165439 (2024).

[57] J.-F. Ren, J. Li, H.-T. Ding, and D.-W. Zhang, Phys. Rev. A **110**, 052203 (2024).

[58] D. C. Brody and E.-M. Graefe, Entropy **15**, 3361 (2013).

[59] D.-J. Zhang, Q.-h. Wang, and J. Gong, Phys. Rev. A **99**, 042104 (2019).

[60] G. Sun, J.-C. Tang, and S.-P. Kou, Frontiers of Physics **17**, 33502 (2022).

[61] C. Chen Ye, W. L. Vleeshouwers, S. Heatley, V. Gritsev, and C. Morais Smith, Phys. Rev. Res. **6**, 023202 (2024).

[62] Y.-C. Tzeng, C.-Y. Ju, G.-Y. Chen, and W.-M. Huang, Phys. Rev. Res. **3**, 013015 (2021).

[63] Y.-T. Tu, I. Jang, P.-Y. Chang, and Y.-C. Tzeng, Quantum **7**, 960 (2023).

[64] A. Fan, G.-Y. Huang, and S.-D. Liang, Journal of Physics Communications **4**, 115006 (2020).

[65] Y.-Q. Zhu, W. Zheng, S.-L. Zhu, and G. Palumbo, Phys. Rev. B **104**, 205103 (2021).

[66] P. He, Y.-Q. Zhu, J.-T. Wang, and S.-L. Zhu, Phys. Rev. A **107**, 012219 (2023).

[67] P. He, H.-T. Ding, and S.-L. Zhu, Phys. Rev. A **103**, 043329 (2021).

[68] Y.-M. R. Hu, E. A. Ostrovskaya, and E. Estrecho, Phys. Rev. Res. **7**, L012067 (2025).

[69] N. Silberstein, J. Behrends, M. Goldstein, and R. Ilan, Phys. Rev. B **102**, 245147 (2020).

[70] J.-H. Wang, Y.-L. Tao, and Y. Xu, Chinese Physics Letters **39**, 010301 (2022).

[71] H. Shen, B. Zhen, and L. Fu, Phys. Rev. Lett. **120**, 146402 (2018).

[72] Q. Liao, C. Leblanc, J. Ren, F. Li, Y. Li, D. Solnyshkov, G. Malpuech, J. Yao, and H. Fu, Phys. Rev. Lett. **127**, 107402 (2021).

[73] J. Cuerda, J. M. Taskinen, N. Källman, L. Grabitz, and P. Törmä, Phys. Rev. Res. **6**, L022020 (2024).

[74] Y.-M. R. Hu, E. A. Ostrovskaya, and E. Estrecho, Opt. Mater. Express **14**, 664 (2024).

[75] A. Mostafazadeh, Journal of Mathematical Physics **43**, 205 (2002).

[76] A. Mostafazadeh, Journal of Mathematical Physics **43**, 2814 (2002).

[77] A. Mostafazadeh, Journal of Mathematical Physics **43**, 3944 (2002).

[78] A. Mostafazadeh, Journal of Physics A: Mathematical and General **36**, 7081 (2003).

[79] J. Pinske, L. Teuber, and S. Scheel, Phys. Rev. A **100**, 042316 (2019).

[80] Y. Chu, Y. Liu, H. Liu, and J. Cai, Phys. Rev. Lett. **124**, 020501 (2020).

[81] G. Rigolin, G. Ortiz, and V. H. Ponce, Phys. Rev. A **78**, 052508 (2008).

[82] C. De Grandi and A. Polkovnikov, "Adiabatic perturbation theory: From landau-zener problem to quenching through a quantum critical point," in *Quantum Quenching, Annealing and Computation*, edited by A. K. Chandra, A. Das, and B. K. Chakrabarti (Springer Berlin Heidelberg, Berlin, Heidelberg, 2010) pp. 75–114.

[83] G. Nenciu and G. Rasche, Journal of Physics A: Mathematical and General **25**, 5741 (1992).

[84] Q. Zhang and B. Wu, Phys. Rev. A **99**, 032121 (2019).

[85] Z.-H. Huang, P. He, L.-J. Lang, and S.-L. Zhu, Phys. Rev. A **107**, 052205 (2023).

[86] R. Wagner, Z. Schwartzman-Nowik, I. L. Paiva, A. Te'eni, A. Ruiz-Molero, R. S. Barbosa, E. Cohen, and E. F. Galvão, Quantum Science and Technology **9**, 015030 (2024).

[87] G. Chiribella, K. Simonov, and X. Zhao, Phys. Rev. Res. **6**, 043043 (2024).

[88] J. Dressel, M. Malik, F. M. Miatto, A. N. Jordan, and R. W. Boyd, Rev. Mod. Phys. **86**, 307 (2014).

[89] H. F. Hofmann, Phys. Rev. Lett. **109**, 020408 (2012).

[90] Y.-L. Wen, Y. Wang, L.-M. Tian, S. Zhang, J. Li, J.-S. Du, H. Yan, and S.-L. Zhu, Nature Photonics **17**, 717 (2023).

[91] D. C. Brody, Journal of Physics A: Mathematical and Theoretical **47**, 035305 (2013).

[92] V. Gritsev and A. Polkovnikov, Proceedings of the National Academy of Sciences **109**, 6457 (2012).

[93] C. Blohmann, The European Physical Journal C **30**, 435 (2003).

[94] F. D. M. Haldane, Phys. Rev. Lett. **61**, 2015 (1988).

[95] Y. Wu, W. Liu, J. Geng, X. Song, X. Ye, C.-K. Duan, X. Rong, and J. Du, Science **364**, 878 (2019).

[96] W. Liu, Y. Wu, C.-K. Duan, X. Rong, and J. Du, Phys. Rev. Lett. **126**, 170506 (2021).

[97] Y. Wu, Y. Wang, X. Ye, W. Liu, Z. Niu, C.-K. Duan, Y. Wang, X. Rong, and J. Du, Nature Nanotechnology **19**, 160 (2024).

[98] Y. Wu, D. Zhu, Y. Wang, X. Rong, and J. Du, Phys. Rev. Lett. **134**, 153601 (2025).

[99] S. Dogra, A. A. Melnikov, and G. S. Paraoanu, Communications Physics **4**, 26 (2021).

[100] U. Günther and B. F. Samsonov, Phys. Rev. Lett. **101**, 230404 (2008).

[101] M. Kolodrubetz, D. Sels, P. Mehta, and A. Polkovnikov, Physics Reports **697**, 1 (2017).